[redacted] PULSED EJECTOR WAVE PROPAGATION TEST PROGRAM

R. Fernandez, J. W. Slater, and D. E. Paxson

The development of, and initial test data from, a nondetonating Pulse Detonation Engine (PDE) simulator tested in the NASA Glenn 1×1 foot Supersonic Wind Tunnel (SWT) is presented in this paper. The concept is a pulsed ejector driven by the simulated exhaust of a PDE. This program is applicable to a PDE entombed in a ramjet flowpath, i.e., a PDE combined-cycle propulsion system. The ejector primary flow is a pulsed, underexpanded, supersonic nozzle simulating the supersonic waves emanating from a PDE, while the ejector secondary flow is the 1×1 foot SWT test section operated at subsonic Mach numbers. The objective is not to study the detonation details, but the wave physics including the starting vortices, the extent of propagation of the wave front, the reflection of the wave from the secondary flowpath walls, and the timing of these events of a pulsed ejector, and correlate these with Computational Fluid Dynamics (CFD) code predictions. Pulsed ejectors have been shown to result in a 3 to 1 improvement in L/D (length-to-diameter) and a near 2 to 1 improvement in thrust augmentation over a steady ejector. This program will also explore the extent of upstream interactions between an inlet and large, periodically applied, backpressures to the inlet as would be present due to combustion tube detonations in a PDE. These interactions could result in inlet unstart or buzz for a supersonic mixed compression inlet. The design of the present experiment entailed the use of an x–t diagram characteristics code to study the nozzle filling and purging timescales as well as a series of CFD analyses conducted using the WIND code. The WIND code is a general purpose CFD code for solution of the Reynolds averaged Navier–Stokes equations and can be applied to both steady state and time-accurate calculations. The first, proof-of-concept, test entry (spring 2001) pressure distributions shown here indicate the simulation concept was successful and therefore the experimental approach is sound. Future testing (planned for mid 2002) will serve to quantify the unsteady ejector performance.

NOMENCLATURE

A_p	primary flow stream cross-section area at mixing region entrance
A_s	secondary flow stream equivalent circular cross-section area at mixing region entrance
D	ejector diameter
D_p	primary flow stream cross-section diameter at mixing region entrance
D_s	secondary flow stream equivalent circular cross-section diameter at mixing region entrance
f	primary nozzle frequency
L	generic length
M_D	detonation Mach number
$\mathrm{M}_{\mathrm{noz}}$	Mach number of the nozzle exit
M_o	free-stream Mach number
M_p	primary stream Mach number
M_s	secondary stream Mach number
P_a	ambient pressure
P_{exit}	pressure at nozzle exit
$P_{t\mathrm{O}}$	local total pressure
P_{pt}	primary nozzle total pressure
t	time (seconds)
T_{ad}	local adiabatic supercooling temperature (Rankine)
T_{dp}	local dew point temperature
T_{O}	ambient total temperature
T_{pn}	primary nozzle total temperature
T_s	local static temperature
w_p	primary stream mass flow
$w_{p\,\max}$	primary nozzle peak instantaneous mass flow
w_s	secondary stream mass flow
x	axial distance
β	ejector entrainment ratio; secondary mass flow to primary mass flow
ϕ	equivalence ratio; $(\text{fuel–air})/(\text{fuel–air})_{\text{stoich}}$

1 BACKGROUND AND INTRODUCTION

The focus of the test program described in this paper is the design and first exploratory run of an attempt to create a noncombusting simulation of a repeating series of shock waves exiting a detonation tube into an enclosing chamber that has forced subsonic flow entering the upstream end and the combined streams exiting out the downstream end of the chamber. No attempt is made to actually simulate the chemical reactions, the exhaust products, or the heat

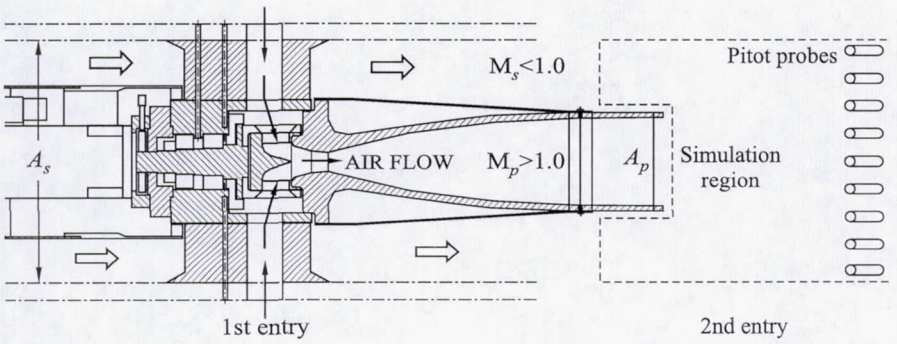

Figure 1 Simulation region: 1st entry: $A_s/A_p = 10$, $D_s/D_p = 3.1$; 2nd entry: $A_s/A_p = 31.2$, $D_s/D_p = 5.6$

release of the detonating wave. The simulation zone starts after the exit of the PDE simulator nozzle and includes the walls of the enclosing chamber, the upstream flow entrance plane, and the downstream mixed flow entrance plane (Fig. 1). Because the detonation chamber is excluded from the simulation, there is no need to reproduce the internal von Neumann pressure spike, nor the thrust generating "plateau" pressure. The parameters that are simulated in the present experiment include: the cycle time or frequency of the disturbances, the detonation tube exit Mach number, a conically shaped (not spherical) shock wave propagating through the confining chamber, the shock reflections off the confining walls, and the associated shock-induced static pressure increases. This simulation should generate any "starting" vortices created, and mixing in the shear layer between the upstream forced flow and the supersonic tube exit.

A pulse detonation engine [1] operates by introducing a fuel–oxidizer mixture into a pressure vessel with an open end and initiating near-constant volume combustion via a detonation. The higher-than-ambient pressure pushing on the closed end of the pressure vessel produces the thrust. An ejector works via the transfer of energy from the primary, or "driving" stream, into the secondary, or "driven" stream. The mixed flow of the two interacting fluid streams exhausts out of the propulsion system at a higher thrust than that of the primary stream alone, i.e., thrust is augmented. The concept discussed in this paper is based on a combination of both concepts to get the greater thermodynamic cycle efficiencies of the PDE when compared to the Brayton cycle with the thrust augmentation of an ejector. This concept involves replacing the traditional steady ejector primary with a PDE and, thus, employing an unsteady ejector system. Pulsed ejectors have been shown to result in a 3 to 1 improvement in L/D and a near 2 to 1 improvement in thrust augmentation [2].

Many studies have been conducted and papers published on PDE concepts during the last decade. The motivations for all these studies are the promises of lighter weight, high efficiencies, and less complexity (i.e., more robust) [3] than turbine engines. The near-constant volume combustion due to the detonation process [4] produces a higher ideal thermodynamic cycle efficiency for a PDE cycle compared to a Brayton cycle. A PDE system compared to a typical turbomachine has far less moving parts and, thus, far less weight and complexity. Compared to turbojets, PDE systems may offer a reduction in development time, a reduction in engine costs, better thrust-to-weights at higher Mach numbers, decreased parts count, and simplified geometry as well as more flexibility when integrating the propulsion system into the airframe. A PDE propulsion system compared to a ramjet propulsion system has similar levels of lightweight and simplicity but has the added benefit of being able to generate static thrust [5].

Pulse detonation engines may be applicable to a broad range of civil aeropropulsion needs — access-to-space, high-performance aircraft, and Unmanned Air Vehicles (UAVs). Figure 2 shows a possible PDE–ramjet combined-cycle engine configuration for a Single Stage-To-Orbit (SSTO) application using a notational reference vehicle.

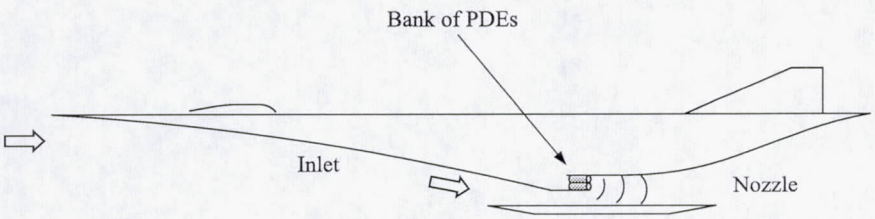

Figure 2 Notional PDE-based combined cycle vehicle

To capitalize on the significant performance benefits of a PDE system, the technical challenges of material limits, combustion-product chemistry, and demonstrated propulsion system component (i.e., vehicle inlet and nozzle, controls, etc.) performance have to be addressed. Material thermal limits [6] and the impact of dissociation and sensible heat release on engine performance [7] have been covered in other papers. Here, the wave propagation information is applicable to how far upstream the interactions between an inlet and large, cyclically applied, backpressures to the inlet, caused by the combustion tube detonations propagating through the mixing section, propagate. For a supersonic mixed-compression inlet, large interactions can result in inlet unstart or buzz.

2 OBJECTIVE

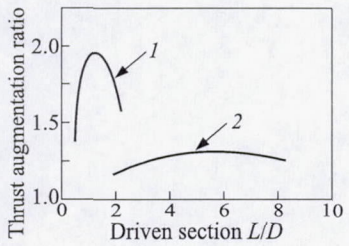

Figure 3 Lockwood's data on comparative thrust augmentation by ejectors [8], area ratio = 10: *1* — pulse jet, and *2* — steady flow

A primary objective of this study is to understand the wave physics of a pulsed ejector including the extent of propagation of the wave front, the reflection of the wave from the secondary flowpath walls, and the timing of these events in order to validate CFD code predictions. The experiment will also quantify the pulsed ejector performance (i.e., thrust augmentation) for this configuration and will be compared to previous studies (Fig. 3) [8]. These past studies show that pulsed ejectors result in a higher thrust augmentation ratio and smaller length-to-diameter ratios than steady state ejectors.

This current test program is one of several studies at the Glenn Research Center (GRC) focused on verifying and understanding unsteady ejector behavior. These various studies encompass the speed regime from subsonic pulsejet-driven ejectors, supersonic pulsed air-jet ejectors (the present paper), to actual PDE-driven pulsed ejectors. The objective being to understand and differentiate the various fluid dynamic phenomena involved in pulsed ejectors. This current test hardware is ideally suited to study pulse or wave shape effects on unsteady ejector performance via the variation of: pulse Mach number, pulse frequency, pulse wave width (via different selections of valve duty cycle), primary-to-secondary area ratios, and primary-to-secondary density ratios.

This test program will also provide data to assess how unsteady downstream conditions affect the performance and operation of inlets. Because inlets are designed to avoid operations near buzz, this dynamic downstream disturbance represents a whole new technology area for inlet designs.

This fundamental experimental program is being conducted in the 1×1 SWT and requires operation in subsonic conditions; a regime outside of the facility design. Therefore during this program the flow quality, both spatially and temporally, of the 1×1 SWT operating in subsonic mode was quantified and the control of the tunnel in this mode was assessed.

3 MODELING

3.1 Nozzle and Valve Design

The primary stream supersonic nozzle design was challenging due to several constraints:

(1) The need to produce supersonic exit Mach numbers at the exit of the nozzle equivalent to those produced by a detonation tube;

(2) The desire to match the geometric configuration of Lockwood (10-to-1 secondary-to-primary area ratio);

(3) A test facility supply pressure limitation for the primary stream of 465 psia and a supply mass flow limitation of 8 lbm/s;

(4) The wind tunnel itself, the secondary stream, has a low-end static pressure limit at the subsonic Mach numbers governed by the geometry of the installed hardware (and its associated pressure losses induced in the tunnel) and the lower limit the valve control system can hold;

(5) Dew point temperatures on the primary stream low enough to prevent condensation in the nozzle; and

(6) The need for a sharp pressure spike or pulse at the nozzle exit; vs. gradual ramp-ups or ramp-downs which would not properly simulate a PDE.

The first test entry's supersonic nozzle was designed for an exit Mach number of 5.0; a hydrogen–oxygen detonation wave generated with $\phi = 1.0$, $T_O = 536.4$ °R, and a $P_{tO} = 14.7$ psia, produces an actual detonation tube exit Mach number (M_D) of 4.83. Figure 4 presents CFD pressure contours of a detonation wave at the above conditions, with a superimposed sketch of the axisymmetric, or conical, underexpanded nozzle shock plume. The second test entry will also include nozzles designed for lower Mach numbers and different ejector area ratios. The combination of the predefined exit Mach number, and the 10-to-1 secondary-to-primary area ratio (the 1×1 SWT's cross-section area equals to 144 sq. in.) defines the supersonic nozzle throat area. With this set, the system mass flow is automatically set for a given pressure. High nozzle Mach number limits are set by the starting pressure ratio needed, with 465 psia being the upstream maximum pressure obtainable, although after flowing through the air valve, the maximum pressure available to the nozzle is about 323 psia. The downstream minimum pressure available is 1.9 psia, although locally lower static pressures are obtainable with the secondary stream flowing. The dew point limit of 445 °R or less is to avoid condensation. The low nozzle Mach number limit is set by the maximum mass flow limit of 8 lbm/s; if the 10-to-1 ejector area ratio is preserved, then the nozzle throat gets larger with decreasing Mach number.

The ejector primary's Mach 5 nozzle was designed with a Method of Characteristics (MOC) FORTRAN code that allows inputs of exit Mach, the ratio of specific heats, γ, and the throat radius. This produces an ideal inviscid nozzle contour that then can be modified to account for boundary layer displacement thickness growth. Because of the small scale of this hardware, there was not a significant change in the nozzle contour due to boundary layer build up. Most

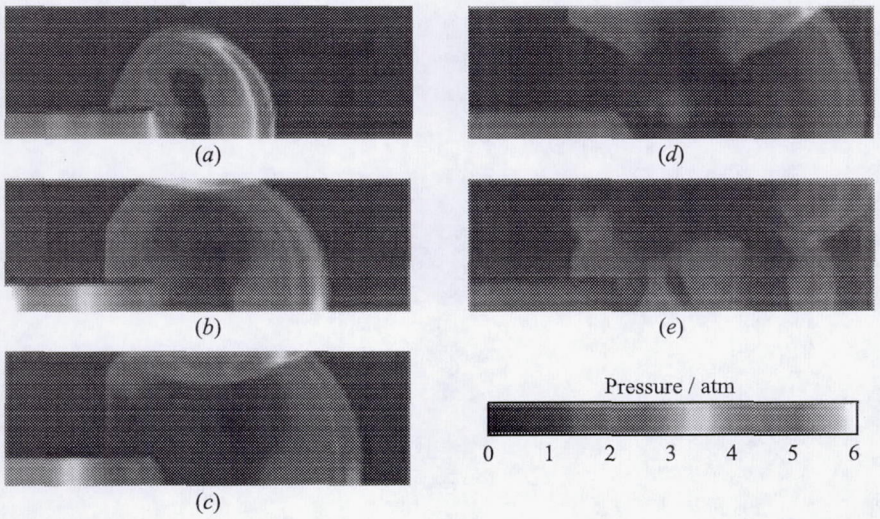

Figure 4 CFD pressure contours of hydrogen/oxygen detonation exiting the PDE tube: (*a*) $t = 0.087$ ms; (*b*) $t = 0.115$ ms, the shock reflects off the tunnel wall; (*c*) $t = 0.142$ ms, the reflected shock has propagated further along the tunnel centerline; (*d*) $t = 0.170$ ms, there is interference between shock waves and expansions; and (*e*) $t = 0.198$ ms. At $t = 0.0188$ ms, the detonation is at the PDE tube exit plane. (Refer color plate XXX.)

of the viscous contour offset was smaller than typical machining tolerances until the very end of the nozzle. Therefore, for the following timescale study and CFD analysis, the original inviscid contour was used.

With the primary nozzle starting pressure ratio (spanning the range of 21 to 200), and the peak primary mass flow of 4.8 lbm/s within bounds, there were three remaining items to be studied: valve duty cycle and the associated nozzle filling and emptying time scales; condensation-induced flow breakdown within the nozzle; and the valve performance requirements.

3.2 Timescale Study

In order to arrive at an estimate of the filling and purging process of the supersonic primary nozzle, which determines the pulse wave shape, a quasi-one-dimensional x–t diagram FORTRAN code was run. This computer code will also be used on the other various nozzles to be tested in the facility.

All of the results presented used a 200-point grid and a nondimensional time step of $\Delta\tau = 0.0005$. All of the results to be presented are nondimensional. The

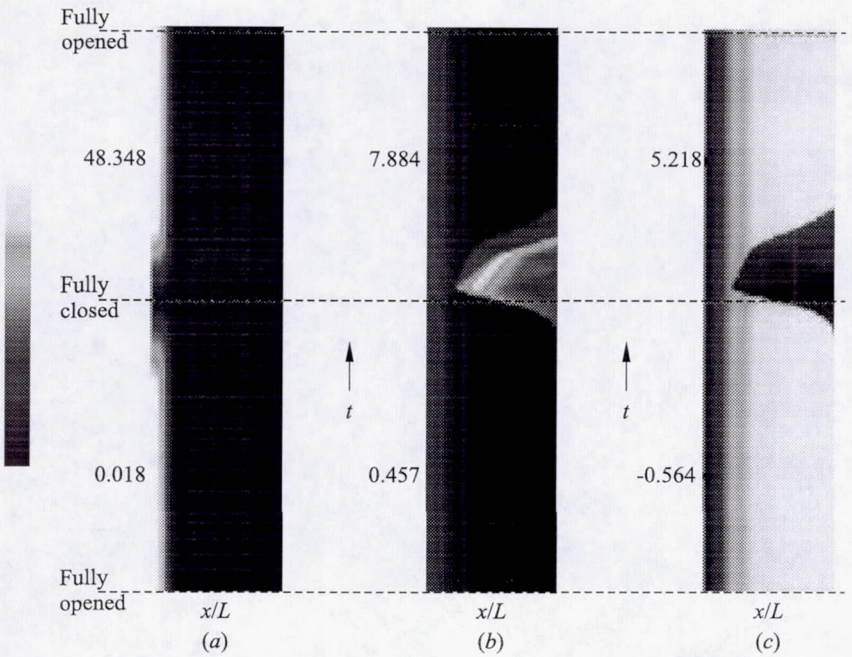

Figure 5 Pressure (*a*), temperature (*b*), and Mach contours (*c*) over one 60-hertz cycle of a Mach 5 nozzle using a linear valve. Numbers beside contours represent high and low values in the x–t space. All values have been nondimensionalized. (Refer color plate XXX.)

Table 1 Reference conditions used to nondimensionalize the Mach 5 nozzle results

p^*, psia	ρ^*, lbm/ft^3	T^*, °R	a^*, ft/s	γ	L, in.
5.75	0.055	281.4	823.0	1.4	16.49

reference conditions used to nondimensionalize the results in Fig. 5 are listed in Table 1.

Because a range of inlet pressure and temperature conditions is tested during the experiment, an average of this range was used as the input. The results are $p_{01} = 287.5$ psia, $T_{01} = 985$ °R. These results are for an overexpanded nozzle with an ambient pressure of $P_a = 10.0$ psia.

Because the quasi-one-dimensional x–t code needs a continuous area distribution, a piecewise curve fit was actually used in the code. The fit was made

using a parabola from $0 < x/L < 0.124$ and a sixth order polynomial from $0.124 < x/L < 1.0$.

3.3 Instantaneous Closing

The first simulation is that of an instantaneous closing of the inlet. Practically, this meant imposing a 'wall' boundary condition on the steady flow and running until the exit flow became subsonic. This turned out to be a very short time. Because of the scaling, it appears that almost nothing is going on until the shock abruptly forms at the exhaust end and travel upstream. In reality, the expansion wave arising from stopping the flow at the inlet end travels down the nozzle. The nozzle is quite underexpanded, with a steady state pressure ratio, P_a/P_{exit} of approximately 19. The expansion wave causes the pressure (P_{exit}) to drop and at $t = 0.27$ (0.45 ms) the pressure ratio exceeds 29, the value corresponding to a normal shock with an incoming Mach number of 5.0.

3.4 Instantaneous Opening

After closing the inlet for the simulation described above, the code was run for an extended period of time. Since there is nothing to damp out waves in the code, they continued to rebound in the nozzle. Thus, at some arbitrary time long after the inlet closing, the inlet was instantaneously reopened. An extrapolation was required due to the way that boundary conditions are imposed in the code. With inflow boundaries, one normally imposes a total pressure and temperature. These values are used, along with characteristic information from the interior of the computing domain, to calculate an appropriate state for the image cell just outside the computing domain. In some situations, such as the instantaneous opening of the nozzle inlet, this approach will show that the entering flow is supersonic, and a Mach number must also be imposed. The Mach number for the image cell was simply specified as 1.0. It makes very little difference however, as this supersonic boundary condition persists for only 0.025 time units (0.04 ms). The flow is essentially sonic at the outlet by 0.27 time units (although it drops slightly below for a period after that). At 1.2 time units, the exhaust flow abruptly jumps to Mach 5 flow.

3.5 Linear Valve at 60 Hz

As a final simulation, a linear valve model that is built into the code was placed at the nozzle entrance. The valve opens linearly to the full size of the inlet and then

closes the same way. The losses associated with the partially open valve appear to be fairly realistic based on previous applications of the code. The results of a simulation of the nozzle with this valve after it has reached limit cycle behavior is presented (Fig. 5), which shows contours of pressure, temperature, and Mach number during this process (an x–t diagram). The horizontal dimension in these figures is the distance along the nozzle, and the vertical dimension is time. The contour plot spans a time equivalent to 1 complete cycle; where the cycle shown is one going from full open (at the bottom of the x–t diagram), to full closed (at the middle of the x–t diagram), to full open again at the top. What is evident in this figure is the fact that while the valve is opening and closing in a linear fashion, the exit flow is generally constant at Mach 5. This is quite different from what comes out of the PDE which is low speed most of the time and high speed only for a very short 'spike.' This result has implications when considering the design of the nozzle valve. For example, when using the spinning valve concept, there is a need to design the slots in the spinning valve such that there is considerably more time spent closed than open, i.e., a small valve duty cycle. For other types of valves, it suggests that a simple sinusoid type drive will not be sufficient to simulate PDE like flows.

3.6 Density Changes via Temperature, Condensation, and Molecular Weight

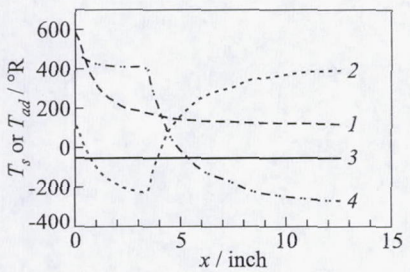

Figure 6 The variation of various temperatures inside the supersonic nozzle: *1* — T_s, *2* — T_{ad}, *3* — −55 limit, and *4* — T_{dp}

An analysis was conducted to determine the local adiabatic supercooling, defined as the cooling of the air below the dew point, along the nozzle's length. An adiabatic supercooling value of less than −55 °R assures that condensation will not occur. Figure 6 shows the variation of local static temperature, T_s, local dew point temperature, T_{dp}, the local adiabatic supercooling, T_{ad}, and the −55-degree Rankine supercooling limit plotted for the test conditions vs. distance traveled along the nozzle. Notice the strong drop in local dew point as the local static pressure drops. This produces a minimum in the supercooling curve that causes the local supercooling problem to go away the further the air travels down the nozzle.

For the first test entry, the primary nozzle air was heated up to 250 °R to generate a density gradient between the primary and secondary air streams, this enhances the flow visualization via shadowgraph and Schlieren techniques.

Side benefits are that the primary stream flow itself will exit relative to the secondary flow ambient temperature at a higher Mach number (~ 2.4) and that condensation in the nozzle will not be an important factor. For the Mach 5 nozzle, with a total temperature of 250 °R, with dew points in the range of -15 to -40 °R (typical run time levels), significant [9] supercooling (i.e., more than $\Delta T = -55$ °R) does not occur until after the flow has traveled 5.6% down the nozzle where it is at approximately Mach 2.1. By then, it takes about 0.5 ms to exit the nozzle; insufficient time to allow significant nucleation [10]. Any water condensation would occur outside of the nozzle, not inside, and so the Mach 5 exit plane condition would be assured. Furthermore, as Fig. 6 indicates, no more nucleation should occur as the air travels down the nozzle and past the minima in the supercooling curve. Since the product of combustion of a "real" H_2–O_2 PDE combined-cycle engine would be water, condensation outside of the primary and into the secondary stream would be acceptable.

In addition to tests of air flowing through the primary nozzle, helium will also be injected through a new primary nozzle and run at the same frequencies. These tests will create a large density gradient between the primary and secondary streams to aid in flow visualization and gather primary-to-secondary density ratio parametric data.

3.7 Valve Performance

The greatest design challenge was the fast-acting rotary air-valve system. Figure 7 shows a typical Mach number and static pressure profile at the exit of a PDE tube for 1 cycle. These profiles represent the features that a valve/nozzle experimental fixture would need to provide and include the von Neumann pressure spike, a plateau pressure level after the spike; and then a decline in the pressure level, that may go subatmospheric until the next detonative pressure spike arrives. Based on this figure, one of the most important features of the valve model and the resultant hardware is a rapid and large build-up of exit pressure followed by its rapid decline. Looking at a series of PDE exit pressure traces from a distance reveals that a series of narrow triangular waves with a large period between them, or a pulse wave with infinitely small peak duration, would make a good approximation of the trace. As is explained in the following section, for the purposes of this study, the actual PDE detonation tube pressure profiles do not have to be reproduced.

Figure 8 shows the actual valve opening area vs. time of the rotary valve scheme depicted in Fig. 9. The axially flowing valve was designed to deliver a pressure spike satisfying the wave shape (depicted in Fig. 8) by: close coupling between the air supply plenum and the valve (to minimize rise times and hysteresis); fast acting between the start of the opening part of the cycle, the full open

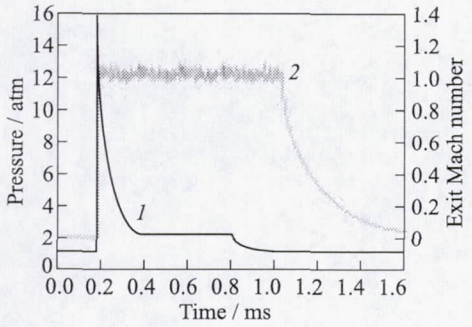

Figure 7 Typical pressure (*1*) and Mach number (*2*) values at the exit of a PDE tube

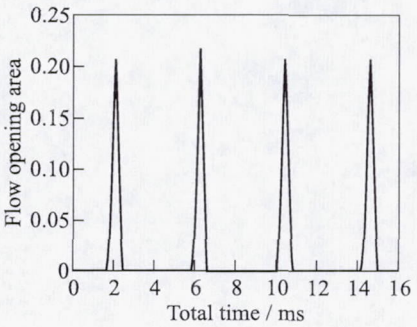

Figure 8 Variation of valve flow area at operating frequency of 240 Hz

peak, and the closing part of the cycle; and close coupling between the valve itself and the supersonic nozzle, again to minimize volume filling and emptying times. The test matrix (Table 2) shows that the pulse frequency was varied at the various test conditions. A significant portion of the data was gathered at 248 Hz. At this operating point, the nozzle will be flowing at Mach 5 for only 0.0009 s (0.9 ms) while for the rest of the 16.13-millisecond cycle, i.e., 0.01523 s (15.23 ms), the nozzle will be either not flowing out or leaking a small amount of flow outwards. Note that Mach 5 is the flow behind the shock wave while the shock wave itself travels through the secondary flow at Mach 1 or less.

4 APPARATUS

4.1 1 × 1-Foot Supersonic Wind Tunnel

The 1 × 1 SWT [11] is a continuous flow facility with test Mach numbers from 1.3 to 6.0. The different Mach numbers are achieved by swapping out the different Mach "blocks" or tunnel nozzles. The upstream high-pressure air is provided by the NASA GRC central air supply service, while the downstream flow is routed to a central exhaust system. The tunnel incorporates an electrical resistance heater to bring the air up to elevated temperature. The air is heated to a high enough temperature to prevent condensation in or liquefaction of the air in the flow. In addition to Mach number and temperature parametrics, Reynolds numbers can be varied via upstream total pressure control. Figure 10 shows the model mounted to the floor and ceiling of the facility test section. The test program

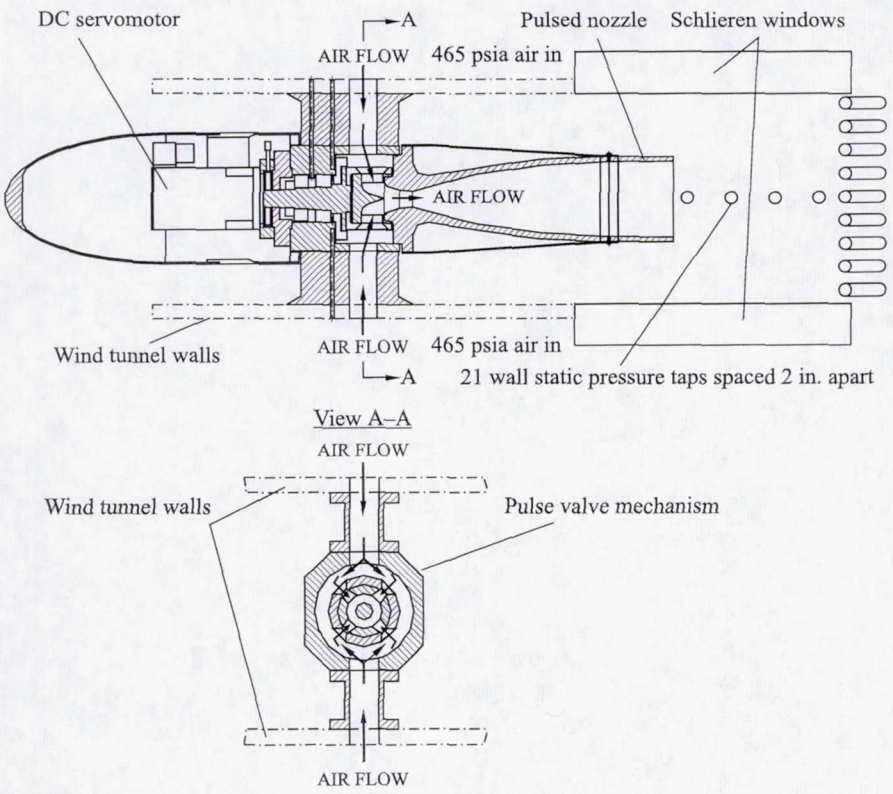

Figure 9 Cross-sectional views of pulse valve mechanism, motor, exhaust nozzle, and wind tunnel walls

used the Mach 1.3 block, with a low enough pressure ratio to assure that the Mach block would not start, i.e., was always operating subsonically. For the picture in Fig. 10, the test section wall has been removed to allow access to the model.

The test methodology is relatively straightforward: the tunnel test flow acts as the subsonic secondary flow and a small supersonic nozzle (the primary flow path) is mounted on tunnel centerline and is pulsed at high frequency. The pulsed shock waves propagating throughout the test section are recorded using high-speed dynamic pressure transducers as well as high-speed Schlieren system and shadowgraph imaging (both film and video were used).

Total pressure measurements were made at the ejector mixing section exit, 14.4 inches aft of the primary nozzle exit. Figure 9 presents a schematic of

Table 2 Condensed matrix of tests in stable subsonic tunnel operating mode (without large-amplitude pressure pulses) at primary nozzle air flow Mach number $M_p = 5$

M_0	H_0, psia	T_{TO}, °R	P_{pt}, psia	T_{pn}, °R	$w_{p\max}$, lbm/s	f
0.43	2.2	534	372.0	531	4.987	Hz sweep
	2.0	525	372.0	526,528,531	4.987	Hz sweep
	1.9	532	—	—	—	Turned off
	1.8	533	—	—	—	Turned off
	1.7	533	372.0	535	4.968	Hz sweep
	1.6	526	372.0	532	4.982	Hz sweep
	1.5	532	398.5	553	5.235	Steady
	1.5	532	390.6	553	5.131	Steady
0.42	2.0	525	372.0	525,526,527,532	4.982	Hz sweep
	1.8	531	140.9	540	1.874	Steady
	1.6	526	372.0	532, 537	4.982	Hz sweep
	1.3	532	404.8	572	5.229	Steady
0.41	2.0	525	372.0	532	4.982	Hz sweep
	1.7	531	140.7	539	1.872	Steady
	1.6	526	372.0	538	4.954	Hz sweep
	1.3	531	386.6	600	4.875	Steady
	1.3	532	393.4	613	4.908	Steady
	1.3	539	398.3	650	4.826	Steady
0.40	1.9	525, 526	372.0	527, 528	5.001	Hz sweep
	1.7	533	—	—	—	Turned off
	1.5	526	372.0	531	4.987	Hz sweep
0.39	1.7	538	372.0	579	4.776	Hz sweep
	1.6	532	—	—	—	Turned off
	1.5	526	372.0	531	4.987	Hz sweep
0.38	1.8	525	372.0	527	5.006	Hz sweep
	1.7	533	393.1	617	4.889	Steady
	1.7	537	372.0	565	4.835	Hz sweep
	1.5	533	372.0	535	4.968	Hz sweep
0.36	1.6	533	9.9	532	0.133	Steady
	1.4	533	372.0	536	4.964	Hz sweep
	1.2	532	149.1	539	1.984	Steady
0.35	2.0	535	372.0	531	4.987	Hz sweep
	1.8	532	396.9	554	5.209	Steady
	1.8	526	372.0	528	5.001	Hz sweep
	1.7	533	—	—	—	Turned off
0.34	2.0	531	372.0	534	4.973	Hz sweep
	1.5	530	138.0	540	1.834	Steady
	1.4	532	90.2	533	1.206	Steady

Continued

Table 2 Condensed matrix of tests in stable subsonic tunnel operating mode (without large-amplitude pressure pulses) at primary nozzle air flow Mach number $M_p = 5$ (*Continued*)

M_0	H_0, psia	T_{TO}, °R	P_{pt}, psia	T_{pn}, °R	$w_{p\max}$, lbm/s	f
0.33	2.0	531	372.0	507 → 535	4.968	Hz sweep
	1.9	534	372.0	528	5.001	Hz sweep
	1.8	528	372.0	527	5.006	Hz sweep
0.32	2.0	531, 534	372.0	508, 532	4.982	Hz sweep
	1.7	525	372.0	527, 531	5.006	Hz sweep
	1.4	532	2.7	532	0.036	Steady
	1.4	532	71.0	533	0.949	Steady
0.31	4.0	532	—	—	—	Turned off
	2.0	533	372.0	529	4.996	Hz sweep
	1.9	534, 535	372.0	531, 527	5.006	Hz sweep
	1.8	530	135.9	540	1.807	Steady
	1.7	525, 527	372.0	526 → 529	4.996	Hz sweep
	1.7	539	—	—	—	Turned off
	1.6	533	5.7	531	0.076	Steady
	1.5	533	—	—	—	Turned off
	1.4	526, 533	372.0	532 → 538	4.982	Hz sweep
	1.1	531	135.4	538	1.803	Steady
	0.9	532	391.4	555	5.132	Steady
0.30	4.1	533	1.6	582	0.021	Steady
	2.0	533	372.0	529	4.996	Hz sweep
	1.8	526	372.0	600	4.691	Hz sweep
	1.4	531	18.6	535	0.249	Steady
	1.4	526	372.0	532	4.982	Hz sweep
	0.9	532	390.1	554	5.120	Steady
	0.7	531	394.0	620	4.888	Steady
0.29	2.0	533	372.0	528	5.001	Hz sweep
0.27	1.7	530	138.9	540	1.846	Steady
0.20	6.0	533	369.4	616	4.598	Steady
	5.7	532	337.1	551	4.436	Steady

Continued

the hardware items and instrumentation locations. In Fig. 10, one of the 1×1 SWT's full span Schlieren windows can be seen below the model. This window is 22.5 inches long and spans the width of the test cabin.

The tunnel was run in a mode (subsonic) outside of its design. Therefore, a calibration of the test section flow was conducted. The tunnel configuration (i.e., nozzle block), total pressure, and flow rate chosen theoretically reflected the combination which provided the most uniform and stable subsonic operation

Table 2 Condensed matrix of tests in stable subsonic tunnel operating mode (without large-amplitude pressure pulses) at primary nozzle air flow Mach number $M_p = 5$ (*Continued*)

M_0	H_0, psia	T_{TO}, °R	P_{pt}, psia	T_{pn}, °R	$w_{p\max}$, lbm/s	f
0.00	1.8	524 → 528	372.0	531 → 545	4.922	Hz sweep
	1.8	530	—	—	—	Turned off
	1.8	530 → 538	372.0	520 → 541	4.941	Hz sweep
	1.5	522 → 528	372.0	524 → 529	4.996	Hz sweep
	1.4	523 → 536	372.0	531 → 619	4.987	Steady
	1.3	525	372.0	516	5.059	Hz sweep
	1.3	531, 530	372.0	534 → 589	4.973	Steady
	0.9	538	402.6	658	4.848	Steady
	1.2	525, 532	372.0	532, 524	4.982	Hz sweep
	1.2	522 → 529	372.0	528 → 545	4.922	Steady
	1.1	532	372.0	531	4.987	Steady
	1.1	526	372.0	542	4.936	Hz sweep
	0.9	531	372.0	545	4.922	Steady
	0.6	531, 532	372.0	546 → 628	4.918	Steady
	0.5	532	372.0	630	4.578	Steady
	0.1	528 → 533	372.0	547, 555	4.878	Steady
	1.2	525, 532	372.0	532, 524	4.982	Hz sweep
	1.2	522 → 529	372.0	528 → 545	4.922	Steady
	1.1	532	372.0	531	4.987	Steady
	1.1	526	372.0	542	4.936	Hz sweep
	0.9	531	372.0	545	4.922	Steady
	0.6	531, 532	372.0	546 → 628	4.918	Steady
	0.5	532	372.0	630	4.578	Steady
	0.1	528 → 533	372.0	547, 555	4.878	Steady

possible; these were verified experimentally. Operational stability was confirmed by adding dynamic pressure transducers along the tunnel during the subsonic calibration of the 1×1 SWT.

4.2 Test Matrix

Table 2 contains the listing of test conditions achieved during the first test entry. Test conditions planned for the second test entry will match these as well as expand the test matrix to higher primary nozzle total pressures when the helium is used. Note that the "Hz sweep" primary nozzle frequency shown in the last column implies that several pulse frequencies were recorded at those conditions. The "steady" term means that the rotary valve was not running and therefore

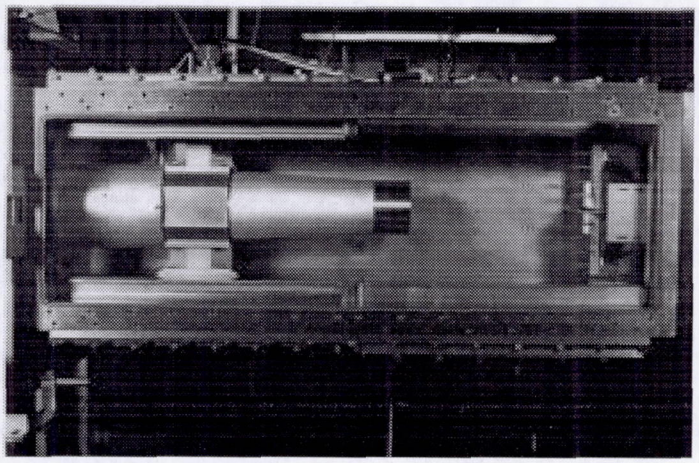

Figure 10 1×1 ft. supersonic wind tunnel test section

steady ejector data was gathered for those conditions. The $w_{p\,\max}$ column refers to the primary nozzle peak instantaneous mass flow, i.e., the mass flow that would occur at the instant the valve reaches its fully opened geometry. The actual mass flow is a time-averaged value dependent on the frequency of operation of the rotary valve.

4.3 Test Hardware and Instrumentation

Although an exact simulation of a pulsed detonation wave train will not be possible with an aerodynamic test, the fact that the simulation region lies outside of the detonation tube means that the von Neumann spike, the plateau pressure, nor the gradual expansion have to be reproduced. The rotary valve and supersonic nozzle combination just have to deliver a periodic pressure spike to the secondary flowpath and the mixing region. Experimental data taken in the NASA GRC's Aero-Acoustic Propulsion Laboratory (AAPL) of a 5-inch PDE acquired by a 15 transducer, 40-foot long instrumentation rake shows that as one travels further downstream of the exit plane, the more the effect of the detonations appears like a pressure spike [12]. The transducer axial locations from the exit of the PDE tube were very similar to those in the 1×1 SWT, as well as the positioning of 5.875 inches from the axial centerline of the PDE tube. In the 1×1 SWT pulsed ejector test, the transducers mounted along the wall were 6 inches from the axial centerline of the primary nozzle. Future comparisons

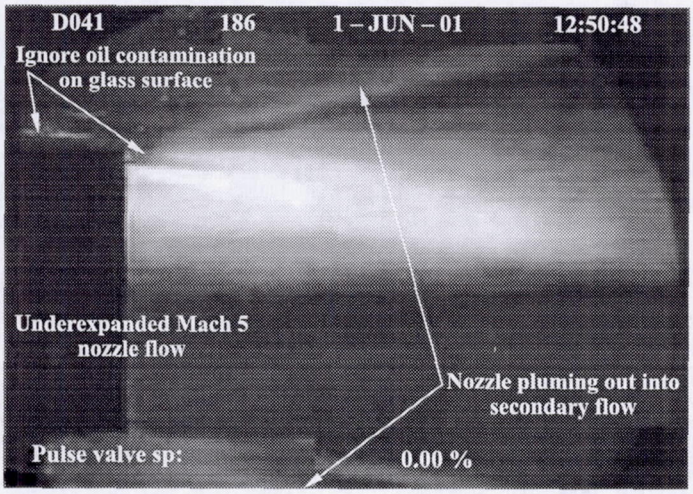

Figure 11 Steady-state ejector Schlieren snapshot

of the pressure spikes, therefore, should be very comparable between the AAPL test and 1×1 SWT test.

Flow visualization was limited to Schlieren and shadowgraph film and video recorded on a high-speed system (a Kodak Ektapro HS video camera at 4000 frames/s and a Phantom Camera at 8000 frames/s). Because it takes a sonic (Mach 1) pulse on the order 0.44 ms to impact the tunnel wall, some of the highest speed systems out on the market were used. The camera remained running afterwards to capture the interference of the shock waves and expansion waves downstream and any subsequent vortex formations. Figure 11 is a snapshot in time of a color Schlieren image taken of the steady underexpanded Mach 5 exit flow to be discussed in the Results and Discussion section of the paper.

5 CFD ANALYSIS AND COMPARISONS

In order to assess the flow quality of the entrance to the secondary flow region, the test geometry was modeled and studied via CFD. An initial concern was what effect a small step in the hardware fairing would have on the flowfield behind it. A long-term goal of this program is to grid the entire model geometry and perform time-accurate CFD of the entire test setup to support unsteady ejector studies.

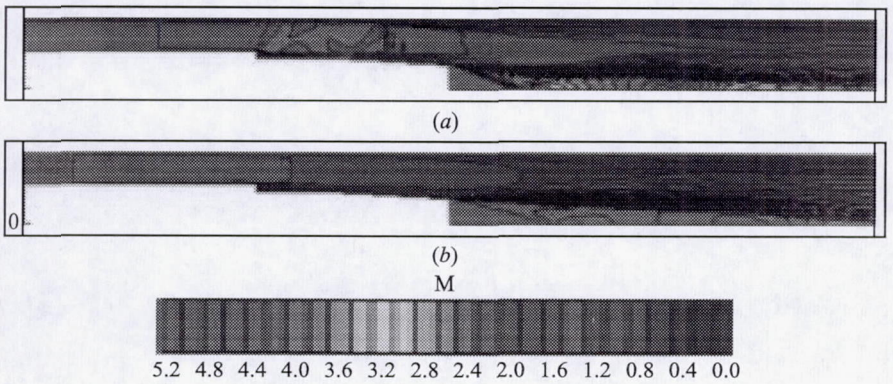

Figure 12 Calculated Mach contours for cases A1 (a) and B1 (b) with the nozzle flow on. (Refer color plate XXX.)

The 1×1 Pulse Ejector Wave Propagation Model has been analyzed using the WIND 3.0 CFD code [13] assuming a planar, axisymmetric flow domain. The objective was to gain a general insight to the flow field about the external surface of the model and test section of the 1×1 SWT with and without flow through the nozzle.

The analysis used a planar flow domain to model axisymmetric flow about the axis of the nozzle. Figure 12 shows the flow domain. The "top" of the flow domain is the tunnel wall. The tunnel cross-section is a 1×1 sq. ft. For the axisymmetric analysis, an assumption is made that the tunnel cross-section is circular with an area of 144 sq. in. The $x = 0$ coordinate is at the nozzle exit. The inflow boundary is located at $x = -40$ in. The downstream/outflow boundary is located at $x = 40$ in. The exterior of the model is at the "bottom" of the flow domain, ahead of the nozzle exit. The "step" in the exterior profile can be seen with a tapering of the radius to the nozzle exit. Ahead of the "step," a straight duct is used rather than trying to model the "bullet" shape of the forward fairing. This approximation is valid as long at the total pressure and total temperature are maintained at the inflow.

The cases examined in this study and the flow conditions of the tunnel and nozzle are summarized in Table 3. $P_{t\mathrm{O}}$ and $T_{t\mathrm{O}}$ are the total pressure and total temperature of the tunnel, respectively. P_{exit} is the flow domain's downstream exit plane static pressure boundary condition.

Case A1 results in an overexpanded nozzle. Case A2 is for the nozzle off. Case B1 is a slightly underexpanded nozzle.

Figure 12 shows the Mach number contours for cases A1 and B1 with the nozzle flow on. Figure 13 shows the Mach number contours for case A2 with

Table 3 CFD cases, tunnel and nozzle conditions

Case	P_{tO}, psi	T_{tO}, °R	P_{exit}, psi	M_{noz}	P_{tnoz}, psi	T_{tnoz}, °R
A1	2.5	520	1.9	5	350	450
A2	2.5	520	1.9	off	off	off
B1	1.25	520	1.75	5	445	860

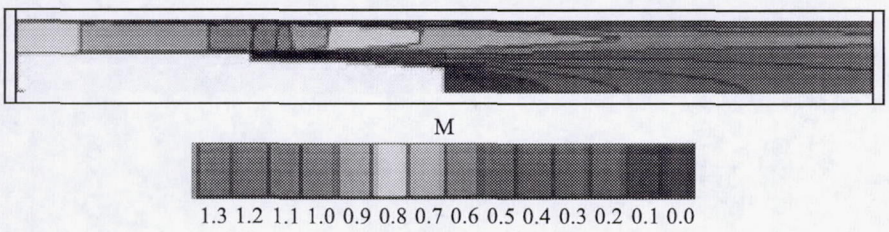

Figure 13 Calculated Mach contours for case A2, the analysis with the nozzle off. (Refer color plate XXX.)

the nozzle flow off. The Mach number contours for cases A1 and A2 indicate a slight local acceleration to supersonic Mach number of the flow past the step. The flow field for case A1 indicates the acceleration of up to Mach 1.5. A fairly strong normal shock develops which results in shock/boundary layer interactions and boundary layer separation on the tunnel wall and model exterior. The flow field for case A2 without the nozzle flow indicates the acceleration of up to Mach 1.1, but little flow separation is noticed. Both flow fields indicate a separation region aft of the "step;" however, the flow seems to reattach and become well developed as it flows down the model exterior toward the nozzle exit. Both simulations A1 and A2 draw the same mass flow from ahead of the nozzle exit, 0.1746 slug/s. When the nozzle flow is on, an additional mass flow of 0.2109 slug/s is added to the test section outflow. The flow field with the nozzle on indicates an overexpanded nozzle flow. The shock train is resolved in a fair manner. The simulation with the nozzle off assumes a solid wall at the nozzle exit. The flow field indicates a separation region at the nozzle exit. The flow field for case B1 indicates that the flow past the step remains subsonic; the mass flow drawn from ahead of the nozzle exit is 0.0812 slug/s. The nozzle flow adds another 0.1928 slug/s. The conclusion of this CFD study is that the presence of the step does not seriously affect the flow at the nozzle exit.

6 RESULTS AND DISCUSSION

6.1 Tunnel Calibration

Figure 14*a* presents the measured tunnel total pressure recovery distribution across the width of the test section, at the 46.40-inch axial station, where the pitot pressure rake has been placed midway between the ceiling and floor of the test section. Presented in Fig. 14*b* is similar data across the height of the test section at the same station, where the pitot pressure rake has been placed midway between the left and right walls of the test section. Varying the upstream supply pressure and the downstream exhaust pressure changed the Mach number. The pressure ratio scale has been expanded to distinguish between the different free-stream Mach numbers, but careful inspection reveals that for all of the Mach numbers, total pressure recovery varies 2.5% or less around the mean value.

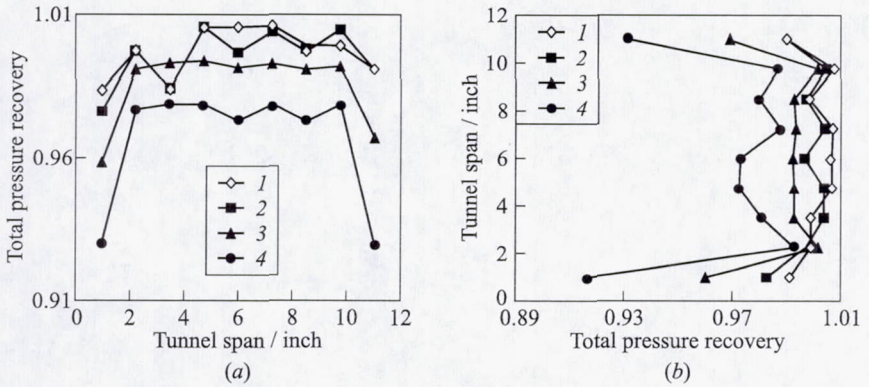

Figure 14 Total pressure distribution at tunnel station 46.4 inch: (*a*) vertical centerline, total pressure divided by upstream total pressure, (*b*) horizontal centerline, total pressure divided by upstream total pressure. *1* — $M_0 = 0.22$; *2* — 0.3; *3* — 0.5; and *4* — $M_0 = 0.7$

6.2 Pulsed Ejector

Because of load problems with the valve's mechanical drive system, the pulsed ejector was only run in the overexpanded mode for these series of "shake out" runs. When the nozzle upstream total pressure reached values of 180 psia or more, the drive system would start slowing down and eventually stop. Several "pulse starts" were performed where the valve was set to a specific frequency with no flow and then the upstream high-pressure air was abruptly turned on. Although these pulse starts did provide 1 to 2 cycles of pressure levels greater

than the 180 psia value, they were not enough to get a series of repeatable underexpanded pulsed ejector data. The thrust loads as well as frictional loads greater than the servomotor could overcome were the cause. The rotary valve did provide very repeatable data for all the overexpanded pulsed ejector cases, but with minimal flow entrainment.

6.3 Steady-State Ejector

Figures 15 and 16 present time histories of data down the wind tunnel, the ejector secondary, for 4 discrete points as an initial screening of the ejector concept for use in future tests. These 4 discrete points are: the far upstream supply piping and plenum (portrayed as station 0 in the plot), the station 4 inches upstream of the primary exit plane, the station at the primary nozzle exit plane, and the pitot pressure rake assembly placed at the 46.35-inch station (i.e., approximately 16 inches downstream from the primary exit). Additional stations were measured but these 4 highlight the important results. The 3 cases presented in the figures are for: an overexpanded nozzle, a fully expanded nozzle, and an underexpanded nozzle. All the data in both figures have been area-averaged by the local flow area at that discrete point. For both figures, the secondary air has been turned off, the wind tunnel piping remains closed, and the primary ejector Mach 5 nozzle is pumping the wind tunnel and test section itself.

Figure 15 presents the local mass flow down the duct for the 3 cases mentioned above. For all 3 cases, the far upstream instrumentation, the $x = 0$ inch station,

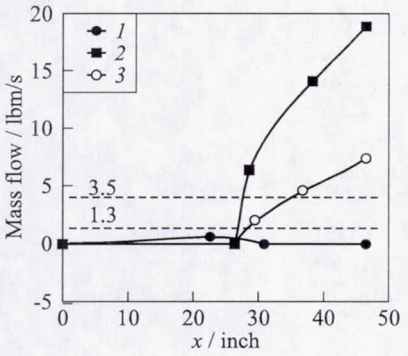

Figure 15 Measured area-averaged local mass flow down the secondary duct: *1* — overexpanded nozzle with p = 1.5 psia; *2* — fully expanded nozzle with p = 1.2 psia; and *3* — underexpanded nozzle with $p = 0.1$ psia

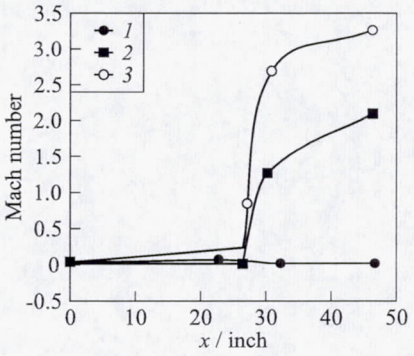

Figure 16 Measured area-averaged local Mach number down the secondary duct: *1* — overexpanded nozzle with p = 1.5 psia; *2* — fully expanded nozzle with p = 1.2 psia; and *3* — underexpanded nozzle with $p = 0.1$ psia

confirms that the forced secondary flow was indeed turned off as no appreciable flow was measured. The second station point shows that while some flow is starting to be pumped down the duct it is still not significant for all three cases. The third point is where the differences start to show. This is the point at the nozzle exit plane where significant pumping is being produced by the underexpanded and fully expanded cases. The overexpanded case shows very little pumping throughout the 4 stations. Also plotted on the figure are the primary stream's mass flow rate; 1.3 lbm/s for the overexpanded case, and 3.5 lbm/s for the fully expanded and underexpanded cases. This is where the area-averaging penalty is noticeable. Because the 1.3 lbm/s was produced by a narrow overexpanded jet that did not expand throughout the secondary region, its area-averaged mass flow was reduced. The last station shows that on an area-averaged basis (and for this quasi-steady case), significant secondary flow was being entrained by the primary stream for the fully expanded and underexpanded jets.

An important point to note is that the fully expanded case with its high entrainment ratio, $\beta = w_s/w_p$, of 4.4 at the pitot rake station was not sustainable. Because the upstream side of the wind tunnel was closed off, the mechanism that occurred is that the ejector evacuated all of the air in the upstream end of the circuit and the static pressure in the test section gradually dropped as the air density dropped. This is consistent with the lack of mass conservation in Fig. 15; there was no conservation of mass in the system since more air was being pumped out than was being put in. Eventually the static pressure dropped enough that the primary nozzle became underexpanded and the stream plumed out throughout the secondary flowpath. The underexpanded entrainment ratio of 1.1 was partially due to the fact the density of the secondary air was significantly reduced because the test facility had been pumped down by the ejector.

Figure 16 shows the local Mach number down the duct for the corresponding three cases. As is shown, the secondary stream itself became supersonic just ahead of the primary exit due to the significant ejector pumping effect.

7 CONCLUDING REMARKS

Based on the results of the tunnel calibration and preliminary "shake out" wind tunnel tests, the concept of a noncombusting PDE simulator as the driver in the study of pulsed ejectors appears to be valid. The wind tunnel calibration results indicate that the use of the tunnel test section itself as the secondary subsonic flowpath was successful for flow uniformity and stability criteria. The supersonic nozzle design as the ejector primary was validated for the steady-state ejector case with significant pumping potential indicated by the pressure data. The mechanical concept for the rotary valve, in which the flow is shut off and periodically opens to allow a fully flowing nozzle, appears to be valid. That the concept is valid was demonstrated with the overexpanded cases where

shock waves were generated and the frequencies were swept from 0 to 400 Hz. The one unknown, currently, is the choice of a large enough motor to overcome the frictional forces in the valve mechanism and the thrust load generated by the fully flowing underexpanded nozzle. With the driving motor problem solved, data will be available to compare this "aerodynamic" simulator of a PDE-driven ejector with actual PDE-ejectors and CFD studies. After the second round of tests are finished, this facility will be available to perform parametric studies on pulse or wave shape affects on unsteady ejector performance via changes to: pulse Mach number, pulse frequency, pulse wave width, primary-to-secondary area ratios, and primary-to-secondary density ratios. Because this is a cold-flow facility with the associated lower costs in instrumentation, model hardware, and test utilities than a hot-fire facility, it is envisioned that phenomena of interest observed in either CFD or more limited PDE hot firings can be studied in detail.

REFERENCES

1. Bussing, T. R. A., and G. Pappas. 1994. An introduction to pulse detonation engines. AIAA Paper No.-94-0263.
2. Lockwood, R. M. 1959. Investigation of the physics of energy transfer from an intermittent jet to an ambient fluid: Summary report. ARD-236, Hiller Aircraft Corp.
3. Bratkovich, T. E., and T. R. A. Bussing: 1995. A pulse detonation engine performance model. AIAA Paper No. 95-3155.
4. Bussing, T. R. A., J. B. Hinkey, and L. Kaye. 1994. Pulse detonation engine preliminary design considerations. AIAA Paper No. 94-3220.
5. Kentfield, J. A. C. 2000. The impact and potential of nonsteady flow phenomena in propulsion and elsewhere. Ohio Aerospace Institute presentation.
6. Paxson, D. E. 2001. A performance map for ideal air breathing pulse detonation engines. AIAA Paper No. 2001-3465.
7. Povinelli, L. A. 2001. Impact of dissociation and sensible heat release on pulse detonation and gas turbine engine performance. *15th Symposium (International) on Airbreathing Engines.* ISABE Paper No. 2001-1212.
8. Porter, J. L., and R. A. Squyers. 1979. A summary of ejector augmentor theory and performance, Phase II — Technical Discussion. ONR R-91100/9CR-47A.
9. Pope, A., and K. L. Goin. 1965. *High-speed wind tunnel testing*. New York: John Wiley & Sons, Inc. 56.
10. Wegener, P. P. Gasdynamics of expansion flows with condensation, and homogeneous nucleation of water vapor. Chapter 4.
11. Seablom, K. D., R. H. Soeder, J. F. X. Leone, and M. W. Henry. 1999. NASA Glenn 1-by 1-foot supersonic wind tunnel user manual. NASA/TM-1999-208478.
12. Dittmar, J. H. 2002. Private communications.
13. Bush, R. H., G. D. Power, and C. E. Towne. 1998. WIND: The production flow solver of the NPARC alliance. AIAA Paper No. 98-0935.